Austin Chemical Engineering

Open Access

Austin Publishing Group

Research Article

Synthesis, Spectral, Thermal, Conductivity, Antimicrobial Studies and Molecular Docking of Some Cefpodoxime Complexes of Some Transition Elements

Alaa E Ali*; Tahra Abdelsabour; Gehan S Elasala
Department of Chemistry, Faculty of Science, Damanhour, Damanhour University, Egypt

***Corresponding author: Alaa E Ali**
Department of Chemistry, Faculty of Science, Damanhour, Damanhour University, Egypt.
Email: alaaeali68@gmail.com

Received: March 28, 2024
Accepted: April 26, 2024
Published: May 03, 2024

Abstract

Cefpodoxime metal complexes were prepared and then studied using stoichiometry 1:1 (M:L), elemental analysis, IR, UV, and visible electronic spectra, magnetic susceptibility, and ESR spectra of the Cu (II) complex. It was suggested that the complexes all have octahedral geometry. The complexes' thermal characteristics were looked at. The TGA and DTA curves were used to estimate the kinetic parameters of the dissociation processes. Except in the case of the Hg complex, no residue was seen following the complexes' thermal disintegration, which resulted in the creation of metal oxide. For several bacteria, cefpodoxime complexes outperformed free ligand in terms of biological activity. Molecular docking of Zn-cefpodoxime, as an example of cefpodoxime complexes, was tested with lung cancer protein where sex binding sites were observed of different amino acids.

Keywords: Coordination chemistry; Metal complexes; Cefpodoxime spectral; Thermal analysis; Conductivity; Mössbauer spectroscopy; Biological activity

Introduction

Figure 1 shows cefpodoxime, a third-generation cephalosporin antibiotic. With the significant exclusions of Pseudomonas aeruginosa, Enterococcus, and Bacteroides fragilis, it is effective against the majority of Gram-positive and Gram-negative pathogens. Cefpodoxime prevents the final trans peptidation step of peptidoglycan production in cell walls, which prevents the creation of cell walls. With a 50% absorption rate, its pharmacokinetic profile is well-established. It should be used for uncomplicated urinary tract infections, uncomplicated skin and skin structure infections, and community acquired pneumonia. It received medical use approval in 1989 after being patented in 1980 [1]. Studying the synthesis, characterization, spectral, thermal, and biological activity studies of cefpodoxime and its metal complexes is the primary focus of this article. Ligands play roles in determining the nature e of interactions in target sites, such as DNA, enzymes and protein receptors provide a high diversity for the design of metallodrugs which may prove a therapeutic activity [2-6].

Experimental Section

Cefpodoxime and metal chloride [Cr(III), Mn(II), Fe(III), Co(II), Ni(II), Cu(II), Zn(II), Cd(II) and Hg(II)] were solvated with bidistilled water. The molar amount of the metal chloride salt was reacted with the calculated amount of the ligand with molar ratios (M:L) 1:1. The reaction mixture was refluxed for about 50 min then left overnight, where the formed complexes were filtrated, then washed several times with a mixture of EtOH-H_2O and dried in a vacuum desiccator. The analytical results are given in Table 1. The metal contents were analyzed based on atomic absorption technique using model 6650 Shimadzu-atomic absorption spectrophotometer and complexometric titration with standard EDTA solution using the appropriate indicator as reported [7]. The analysis of chloride contents of the complexes was examined by Volhard method [8].

Physical Measurements

Metal ion content: The complexes, of accurate weight 0.01-0.02 g, then digested and decomposed by aqua-regia solution. The decomposition step was done several times to ensure that all organic matters were completely destroyed. The residue was dissolved in doubly distilled water. The metal contents were determined based on atomic absorption technique using model 6650 Shimadzu-atomic absorption spectrophotometer and examined complexmetrically with standard EDTA solution using the appropriate indicator as reported [7].

C, H, N, S and Cl contents: C, H, N and S contents, for all the synthesized complexes, were recorded on CHNS No. 11042023, at central lab, Cairo University. The analysis of chloride contents of the complexes were determined by applying the familiar Volhard method [8].

Uv.-Vis. electronic spectra: The spectrophotometric mea-

Citation: Ali AE, Abdelsabour T, Elasala GS. Synthesis, Spectral, Thermal, Conductivity, Antimicrobial Studies and Molecular Docking of Some Cefpodoxime Complexes of Some Transition Elements. Austin Chem Eng. 2024; 11(1): 1108.

Table 1: Elemental analysis, melting points and colors of cefpodoxime (HL) complexes.

Calculated/(Found)%						*m.p./ °C	Colour	Com-plexes
Cl	M	S	N	H	C			
12.11	8.88	10.95	11.96	3.44	30.78	294	dark green	$[CrLCl_2(H_2O)_2]$
-11.09	-8.87	-10.93	-11.94	-3.42	-30.75			
11.99	9.28	10.74	11.79	3.56	30.55	280	Buff	$[Mn(HL)Cl_2(H_2O)_2]$
-12.03	-9.32	-10.88	-11.88	-3.59	-30.57			
12.03	9.48	10.88	9.48	3.42	30.58	227	Dark brown	$[FeLCl_2(H_2O)_2]$
-12	-9.47	-10.85	-9.46	-3.43	-30.55			
11.95	9.93	10.81	11.8	3.57	30.37	258	Pink	$[Co(HL)Cl_2(H_2O)_2]$
-11.93	-9.91	-10.78	-11.79	-3.54	-30.36			
11.95	9.9	10.81	11.81	3.57	30.38	273	Pale green	$[Ni(HL)Cl_2(H_2O)_2]$
-11.96	-9.88	-11.79	-11.8	-3.55	-30.36			
11.86	10.63	10.72	11.71	3.54	30.13	282	Green	$[Cu(HL)Cl_2(H_2O)_2]$
-11.83	-10.6	-11.7	-11.68	-3.52	-30.1			
11.82	10.9	10.69	11.68	3.53	30.04	264	White	$[Zn(HL)Cl_2(H_2O)_2]$
-11.8	-10.87	-10.66	-11.65	-3.51	-30			
10.96	17.38	9.91	10.83	3.27	27.86	244	Off white	$[Cd(H_2L)Cl_2(H_2O)_2]$
-10.92	-17.36	-9.88	-10.8	-3.24	-27.84			
9.65	27.29	8.72	9.53	2.88	24.51	230	Off white	$[Hg(H_2L)Cl_2(H_2O)_2]$
-9.63	-27.27	-8.7	-9.5	-2.86	-24.49			

*All melting points pointed to starting fusion since the complexes take a range from 4 to 5°C range to be fused completely.

Table 2: Fundamental infrared bands (cm^{-1}) of cefopodoxime and its metal complexes.

Cefpodox-ime	Cr com-plex	Mn com-plex	Fe com-plex	Co com-plex	Assignments
3440 (b)	3441 (b)	3458 (b)	3410 (b)	3448(b)	ν_{O-H} of H_2O
3000 (w)	2941(w)	2943 (w)	2940 (w)	2945(w)	ν_{C-H}
1795 (s)	1768 (vs)	1767 (s)	1768 (s)	1768(s)	$\nu_{C=O}$ (β- lactam)
1635(w)	1643 (s)	1644 (m)	1645 (m)	1643 (m)	$\nu_{C=O}$ amide
1350 (m)	1310 (vs)	1312 (m)	1325 (s)	1305 (m)	ν_{COO} (asymm)
1500 (m)	1490 (m)	1492 (m)	1492 (m)	1489 (m)	ν_{COO} (symm)
1188 (w)	1185 (w)	1189 (w)	1186 (w)	1186 (m)	ν_{C-N} (β- lactam)
1108 (m)	1107 (s)	1108 (m)	1106 (s)	1109 (s)	ν_{C-O} of methoxy group
1049 (s)	1040 (vs)	1044 (s)	1041(vs)	1049 (vs)	ν_{N-O} of oxime
861 (m)	861 (w)	865 (w)	866 (w)	862 (w)	γ (COO)
788 (w)	789 (m)	788 (w)	790 (w)	789 (w)	ω(COO)
640 (w)	642 (s)	641 (m)	638 (m)	640 (m)	ρ(COO)
------	500(w)	481 (w)	484 (w)	485(w)	υ_{M-O}
------	355 (w)	358 (w)	358 (w)	359 (w)	υ_{M-Cl}
-------	439	437	436	436	υ_{M-N}
1005 (w)	1003 (w)	1009 (w)	1010 (w)	1009	υ_{C-S}

Table 3: Electronic absorption spectra (nm) and room temperature magnetic moment values (μ eff ,298°K) B.M of cefpodoxime complexes.

Cefpodoxime complexes	λ_{max} (nm)	μ_{eff}
Cr^{III} - complex	325, 350, 415, 600	3.88
Mn^{II} - complex	305, 350, 400, 450, 528	5.82
Fe^{III} – complex	335, 510	5.95
Co^{II} complex	295, 350, 540	3.85
Ni^{II} – complex	350, 575	2.81
Cu^{II} – complex	493, 800	1.68

surements in ultraviolet and visible spectra regions were recorded by using a double beam spectrophotometer UV-530, Rev. 1.00, PC (JASCO Corp) mode covering the wavelength range 190-900 nm. Two quartz cells of 1 mm thickness were used, one for the test solution and the other for the blank. The spectra of the solid complexes were measured using nujol mull technique [9].

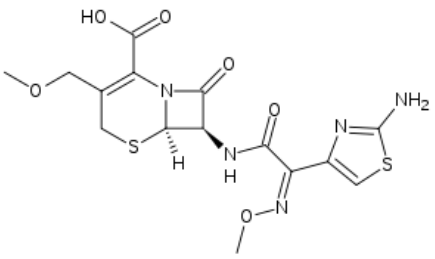

Figure 1: Structure of Cefpodoxime.

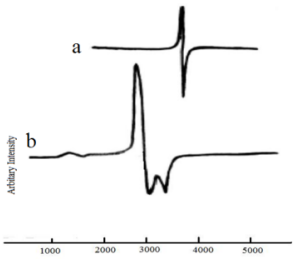

Figure 2: ESR spectrum of: (a) DPPH (b) Cu-cefpodoxime complex.

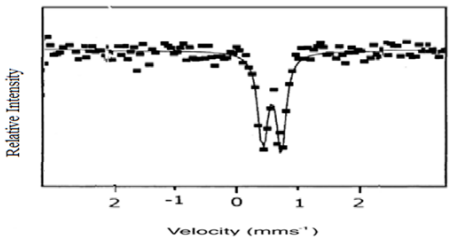

Figure 3: *Mössbauer- Spectroscopy of Fe^{III} cefpodoxime complex.*

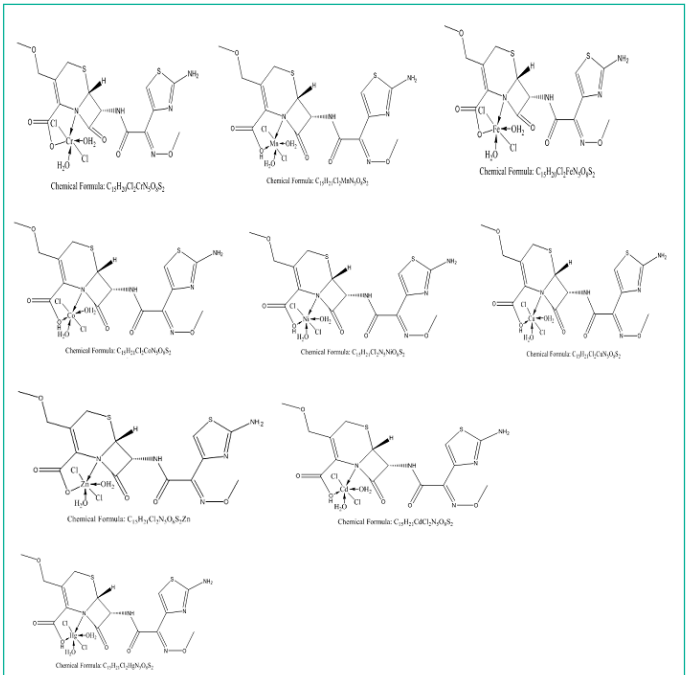

Figure 4: Proposed structures of cefpodoxime complexes.

Infrared spectra: The infrared spectra of the ligands and their metal complexes were taken in potassium bromide disc using Perkin Elmer spectrophotometer, Model 1430 covering frequency range of 200-4000 cm^{-1}. Calibration of frequency reading was made with polystyrene film (1602 ± 1 cm^{-1}).

Electron Spin Resonance spectra (ESR): X-band electron spin resonance spectra were recorded with a reflection spectrometer operating at (9.1-9.8) GHZ in a cylindrical resonance cavity with 100 KHZ modulation. The magnetic field was controlled with a (LMR Gauss meter). The g values were determined by comparison with DPPH signal.

Mössbauer spectroscopy: Mössbauer spectroscopy of iron

Table 4: Room temperature ESR spectral data for copper (II) complexes.

Complex	$g_{\perp}$	$g_{//}$	G	<g>	$A_{//}$	$A_{\perp}$	α^2	f^2
Cu-cefpodoxime	2.263	2.0264	0.00995	2.180	249	25.0	0.85	0.82

Table 5: Kinetic parameters of dissociation steps for cefpodoxime and its metal complexes.

	T/°C	n	β	α	Ea(kJ/mol)	ΔH(kJ/mol)	Z S^{-1}	ΔS (kJ/mol)
Cefpodoxime	40	1.26	2.41	0.59	30.65	-38.07	29.48	-0.12
	80	1.38	2.55	0.57	87.78	-39.55	83.01	-0.11
	161	1.14	2.24	0.61	20.46	-54.60	12.87	-0.13
	417	1.22	2.37	0.59	37.05	-83.11	15.45	-0.12
Cr complex	40	1.78	2.88	0.52	38.33	-37.00	44.46	-0.12
	100	1.15	2.26	0.61	12.41	-48.46	9.14	-0.13
	216	1.82	2.9	0.52	62.06	-55.89	45.67	-0.11
	376	1.37	2.53	0.57	80.35	-73.56	38.55	-0.11
Mn complex	136	1.6	2.75	0.54	21.04	-50.66	17.27	-0.12
	370	1.15	2.26	0.61	63.93	-74.73	27.53	-0.12
	520	1.33	2.5	0.58	108.30	-88.01	41.93	-0.11
Fe complex	96	1.65	2.79	0.54	27.86	-44.77	25.97	-0.12
	190	1.49	2.66	0.56	29.12	-56.22	20.46	-0.12
	316	1.47	2.64	0.56	138.50	-63.76	78.34	-0.11
	429	1.48	265	0.56	135.79	-49.30	6372.96	-0.07
Co complex	82	1	2	0.63	17.25	-45.49	11.88	-0.13
	223	1.63	2.06	0.63	65.31	-57.89	33.68	-0.12
	308	1.53	2.69	0.55	68.06	-66.35	38.83	-0.11
	368	2.75	3.27	0.44	125.44	-68.84	79.84	-0.11
Ni complex	114	1.43	2.6	0.56	22.13	-47.94	18.20	-0.12
	212	1.2	2.33	0.6	28.50	-59.52	16.71	-0.12
	329	1.78	2.88	0.52	14.66	-76.19	8.48	-0.13
	441	2.01	3.01	0.5	112.04	-77.91	58.33	-0.11
Cu complex	122	1.76	2.87	0.52	16.90	-49.51	14.96	-0.13
	214	1.24	2.39	0.59	23.50	-60.45	14.04	-0.12
	340	1.78	2.88	0.52	121.05	-66.65	71.10	-0.11
	450	1.91	2.95	0.51	114.36	-78.89	57.62	-0.11
Zn complex	76	1.05	2.09	0.62	66.29	-40.55	50.98	-0.12
	170	1.06	2.12	0.62	54.06	-52.29	32.16	-0.12
	260	2.33	3.14	0.47	63.15	-60.51	45.96	-0.11
	413	0.64	0.88	0.71	45.91	-87.04	7.17	-0.13
	495	0.78	1.43	0.68	171.30	-85.78	39.72	-0.11
	510	2.39	3.16	0.47	831.42	-71.18	475.05	-0.09
Cd complex	80	1.05	2.1	0.62	27.11	-43.74	19.91	-0.12
	254	1.27	2.43	0.59	91.93	-59.25	53.05	-0.11
	380	1.5	2.67	0.55	39.20	-77.69	19.49	-0.12
	548	0.74	1.29	0.69	32.53	-103.95	6.18	-0.13
Hg complex	95	1.67	2.8	0.53	20.69	-45.57	19.28	-0.12
	160	1.51	2.68	0.55	49.84	-50.56	38.31	-0.12
	315	1.7	2.82	0.53	47.58	-68.71	27.90	-0.12
	504	0.75	1.35	0.68	44.55	-96.03	9.39	-0.12
	576	1.36	2.53	0.57	102.11	-94.58	37.23	-0.11

complexes were recorded at room temperature using a computerized Mössbauer spectrometer MS-1200, model: Ranger in standard transmission geometry with a 20 m Ci Co^{57}(Rh) source. Mössbauer spectra have been analyzed by means of least square computer fitting using Mössfit computer program. The isomer shift values refer to that of metallic iron at room temperature.

Magnetic moment values: Molar magnetic susceptibilities, corrected for diamagnetism using Pascal,s constants were determined at room temperature (298 °K) using Faraday method. The instrument was calibrated with $Hg[Co(SCN)_4]$ [10].

Table 6: The values of conductivity at different temperature for Cr cefpodoxime complex.

T/°C	σοημ^{-1} χμ^{-1}	1000/T (K^{-1})	Ln s
25	4.04x10^{-09}	3.35401641	-19.3259
30	7.70x10^{-09}	3.298697029	-18.6826
35	9.4363x10^{-09}	3.24517282	-18.4787
40	1.50x10^{-08}	3.193357767	-18.0145
45	2.04x10^{-08}	3.143171454	-17.7069
50	2.96573x10^{-08}	3.09453814	-17.3336
55	3.63976x10^{-08}	3.047386866	-17.1288
60	4.3138x10^{-08}	3.001650908	-16.9589
65	4.98783x10^{-08}	2.957267501	-16.8137
70	5.66186x10^{-08}	2.914177473	-16.6869
75	6.3359x10^{-08}	2.872325129	-16.5744
80	7.00993x10^{-08}	2.831657964	-16.4734
85	7.68396x10^{-08}	2.792126214	-16.3815
90	8.358x10^{-08}	2.753683043	-16.2975
95	9.03203x10^{-08}	2.716284126	-16.2199
100	9.70607x10^{-08}	2.679887453	-16.1479
105	1.03801x10^{-07}	2.644453259	-16.0808
110	1.10541x10^{-07}	2.609943886	-16.0179
115	1.17282x10^{-07}	2.576323586	-15.9587
120	1.24022x10^{-07}	2.543558438	-15.9028
125	1.25x10^{-07}	2.511616225	-15.8943
130	1.28x10^{-07}	2.480466328	-15.8751
135	1.31x10^{-07}	2.450079628	-15.8519
140	1.30x10^{-07}	2.420428416	-15.8563
145	1.32x10^{-07}	2.391486309	-15.8378
150	1.35x10^{-07}	2.36322817	-15.8154

Thermal analysis: Differential Thermal Analysis (DTA) and Thermogravimetric Analysis (TGA) of the ligands and their complexes were carried out using a Shimadzu DTA/TGA-50. The rate of heating was 10 °C/min. The cell used was platinum and the dry nitrogen rate flow over the samples was 10 ml/ min. The chamber cooling water flow rate was 10 l/h. the speed was 5 mm/min. Measurements were achieved by applying the baseline methods. Lipped pans were used to eliminate the sloping of the baseline. A Pt 100 thermocouple was used as temperature sensor.

D.C conductivity measurements: The electrical measurements were measured in the temperature range 289–423K. The complexes were prepared in the form of tablets at a pressure of 4-ton cm^{-2}. The tablets were of an area 2.54 cm^2 and thickness 0.12 cm. The samples were hold between two copper electrodes with a silver paste in between and inserted with the holder vertically into cylindrical electric furnace. The potential drop across the heater was varied gradually through VARIAC variable transformer to produce slow rate of increasing temperature to get accurate temperature measurements. The circuit used to measure the electric conductivity consists of D.C. regulated power supply Heat Kit (0–400V), Keith multi-meter for measuring current with a sensitivity up to 10–15A. The temperature of the sample was measured within ±0.1°C by means of copper-constantan T Type thermocouple. This type has excellent repeatability between –380F to 392F (–200°C to 200°C). The conductivity was obtained in the case of cooling using the general formula: $\sigma = I\, d/ V_c\, a$ where 'I' is the current in ampere, V_c is the potential drop across the sample of cross section area 'a' and thickness 'd'.

Table 7: Ln σ_o and ΔEa for cefpodoxime complexes.

	Slope of Ln σ_o – 1000/T relation	Ln σ_o	ΔEa / eV
Cr- complex	-3.55	-6.65	0.000295165
	-0.85	-13.79	7.06733 x10^{-05}
Mn – complex	-1.69	-12.21	0.000140515
	-1.12	-13.6	9.31225 x10^{-05}
Fe – complex	-0.17	-17.76	1.41347 x10^{-05}
	-2.67	-9.50	0.000221997
	-3.19	-8.35	0.000265233
Co – complex	-0.16	-17.81	1.33032 x10^{-05}
	-0.40	-16.79	3.3258 x10^{-05}
Ni – complex	-1.97	-11.81	0.000163546
	-2.14	-10.99	0.000177931
Cu – complex	-0.21	-17.67	1.74605 x10^{-05}
	-2.64	-9.78	0.000219503
	-0.32	-15.54	2.66064 x10^{-05}
Zn – complex	-0.27	-17.44	2.24492 x10^{-05}
	-2.51	-10.02	0.000208694
Cd – complex	-0.10	-18.00	8.31451 x10^{-06}
	-0.53	-16.74	4.40669 x10^{-05}
Hg – complex	-1.97	-11.82	0.000163796
	-2.07	-11.16	0.00017211
	-3.36	-8.00	0.000279368

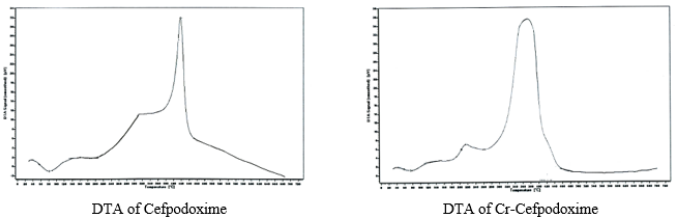

Figure 5: DTA of studied cefpodoxime and its Cr-complex as an example.

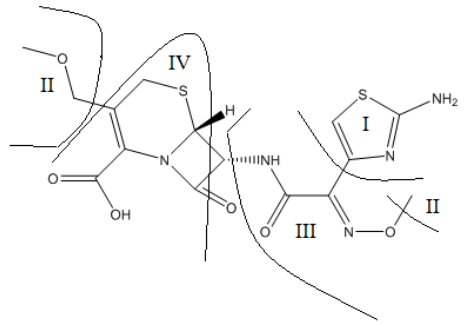

Figure 6: The steps, I-IV of the thermal dissociation of cefpodoxime.

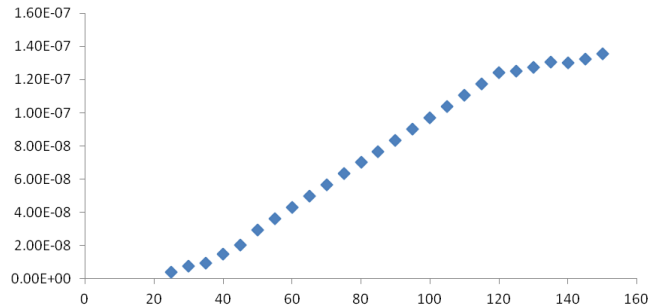

Figure 7: σ relation with T/°C for Cr-cefpodoxime complex.

Dielectric constant, A.C. conductivity, study: The dielectric constant measurements of some selected solid complexes were taken in air on a meter type Hioki 3532 LCR Hitester version 1.02 Japan and cell type (Pw 950/60). Six complexes were pressed into disks of 10 mm diameter and 1-2 mm thickness at a pressure of 9.8 x 10^8 pa. Silver paste was painted on the major faces

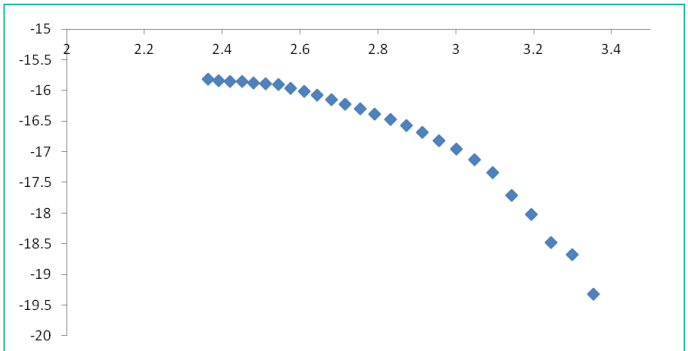

Figure 8: Ln relation with 1000/T/ for Cr-cefpodoxime complex.

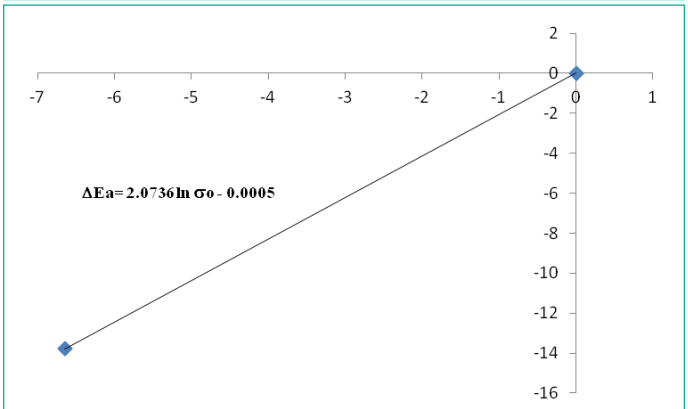

Figure 9: E_a - Ln σ_o for Cr - cefpodoxime complex.

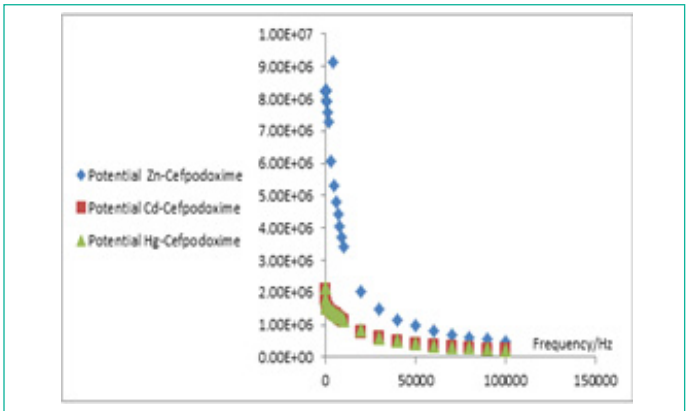

Figure 10: Potential – Frequency relation for cefpodoxime complexes.

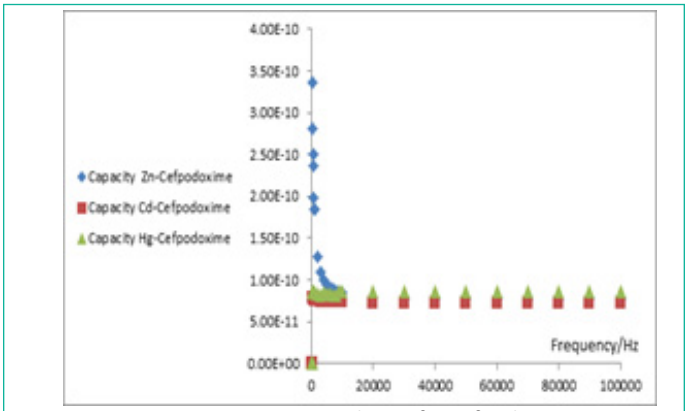

Figure 11: Capacity – Frequency relation for cefpodoxime complexes.

of each tested piece as electrodes. The measurements of the dielectric constant and the dielectric constant were performed in the frequency range 10^2-10^5 Hz at 25ºC.

Biological activity: Antimicrobial activity of cefpodoxime, their metal complexes was determined using the agar well diffusion assay. The tested organisms: *S. pyogenes*, *K. pneumoniae*, *P. mirabilis*, *E. fecalis*, *S. pneumoniae*, *P. aeruginosa*, *E. coli*

Table 8: Antibacterial activity of cefpodoxime, and their metal complexes.

Compounds	S.pyogenes (RCMB010015)	K.pneumoniae (RCMB001009)	P.mirabilis (RCMB010085)	E.fecalis (RCMB010075)	S.pneumoniae (RCMB010029)	P.aeruginosa (RCMB010043)	E.coli (RCMB010056)	S.aureus (RCMB010027)
Cefpodoxime	21.4	21.1	19.7	17.9	21.3	16.7	21.8	23
Cr – cefpodoxime complex	18.3	15.6	14.5	14.8	14.5	14.3	15.2	15.2
Mn- cefpodoxime complex	21.4	20.7	17	15.2	19	14.3	20	20.8
Fe- cefpodoxime complex	16.4	15.2	14.9	14.8	15.5	14.3	15.2	16.5
Co- cefpodoxime complex	12.7	12.2	11.7	9.6	11	14.3	15.2	13
Ni- cefpodoxime complex	22.9	21.2	17.7	16.4	20.3	14.3	20.8	21.7
Cu- cefpodoxime complex	10.4	10	14.9	14.8	10	14.3	15.2	11.8
Zn- cefpodoxime complex	24.9	23.6	22.9	19.9	22.5	19.4	24.2	24.6
Cd- cefpodoxime complex	20	19.1	15.9	14.3	19	14.3	19.3	19.9
Hg- cefpodoxime complex	22.9	21.1	22.1	19	20.9	17.8	22.5	23.3

Table 9: MIC (µg/ml) for antibacterial activity of cefpodoxime, and their metal complexes.

Compounds	A.niger (RCMB2317)	A.flavus (RCMB02426)	S.racemosum (RCMB05922)	C.albicans (RCMB05031)	C.glabrata (RCMB05274)	F.oxysporum (RCMB08213)	R.solani (RCMB09421)	A.solani (RCMB07324)
Cefpodoxime	12.3	13.1	13.3	1.17	11.6	11.9	1.17	9.8
Cr – cefpodoxime complex	19.5	20.6	14.4	1.08	16.3	20.9	0.68	12.75
Mn- cefpodoxime complex	14.5	16.4	14.65	1	15.1	15.2	0.63	12.2
Fe- cefpodoxime complex	9.25	8.3	13.25	0.92	9.3	12	1.03	8.3
Co- cefpodoxime complex	10.15	9.3	11.3	0.83	10.5	12.2	0.99	2.4
Ni- cefpodoxime complex	20	20.9	16.2	0.75	15.3	22.5	0.49	14.55
Cu- cefpodoxime complex	15.3	17.4	13.85	0.67	15.7	15.8	0.44	12
Zn- cefpodoxime complex	15.8	15.3	13.7	0.58	13.55	20.2	0.4	1.3
Cd- cefpodoxime complex	18.5	20.15	16.75	0.5	18.1	20.7	0.35	12.9
Hg- cefpodoxime complex	13.9	12.55	15.55	0.42	12.8	15.5	0.8	1.04

Table 11: MIC for antifungal activity of cefpodoxime and their metal complexes.

Compounds	A.niger (RCMB2317)	A.flavus (RCMB02426)	S.racemosum (RCMB05922)	C.albicans (RCMB05031)	C.glabrata (RCMB05274)	F.oxysporum (RCMB08213)	R.solani (RCMB09421)	A.solani (RCMB07324)
Cefpodoxime	52.6	62.5	31.55	2.1	53.9	64.9	2.05	89
Cr – cefpodoxime complex	0.58	0.49	1.2	1.85	32.25	0.39	1.49	62.45
Mn- cefpodoxime complex	0.09	0.49	1.9	2.3	6.7	0.02	1.06	30.65
Fe- cefpodoxime complex	62.45	62.5	62.45	3.1	124.9	3.8	1.43	1.36
Co- cefpodoxime complex	1.9	0.98	7.8	5.9	1.85	0.39	1.18	62.5
Ni- cefpodoxime complex	3.5	1.95	5.1	5.2	2.8	0.88	1.17	124.95
Cu- cefpodoxime complex	15.23	31.25	15.58	5.7	61.4	1.85	1.9	2.05
Zn- cefpodoxime complex	7.41	1.95	59.8	62.2	1.9	1.69	1.9	1.35
Cd- cefpodoxime complex	3.5	1.9	7.75	3.7	2.8	0.88	1.65	124.4
Hg- cefpodoxime complex	1.81	0.19	0.93	2.7	1.85	2.4	2.6	15.63

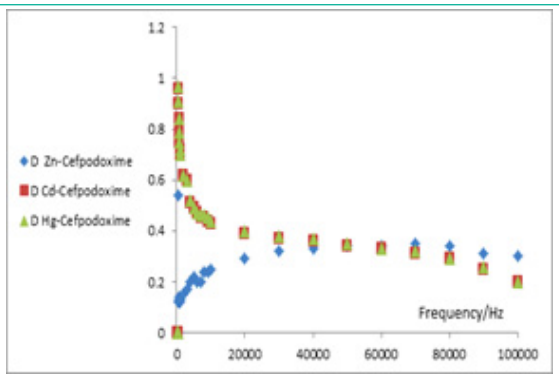

Figure 12: Dielectric Constant – Frequency relation for cefpodoxime complexes.

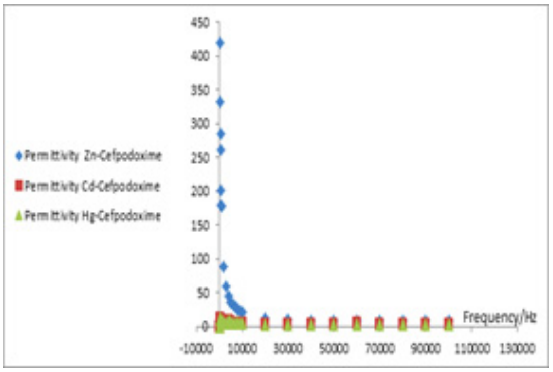

Figure 13: Permittivity – Frequency relation for cefpodoxime complexes.

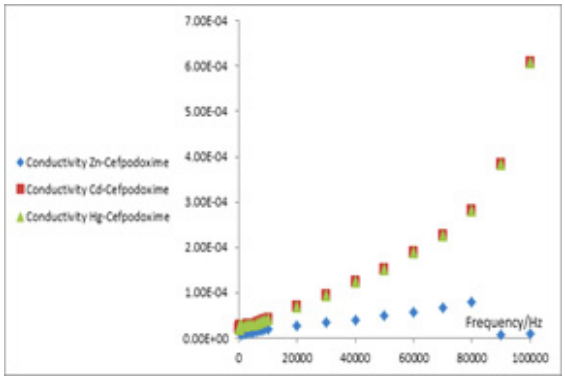

Figure 14: Conductivity – Frequency relation for cefpodoxime complexes.

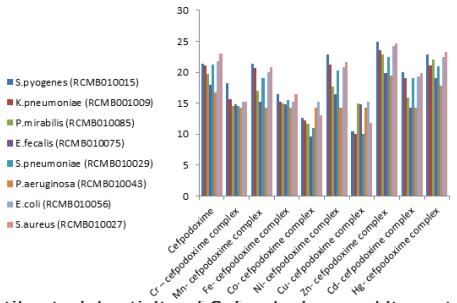

Figure 15: Antibacterial activity of Cefpodoxime and its metal complexes.

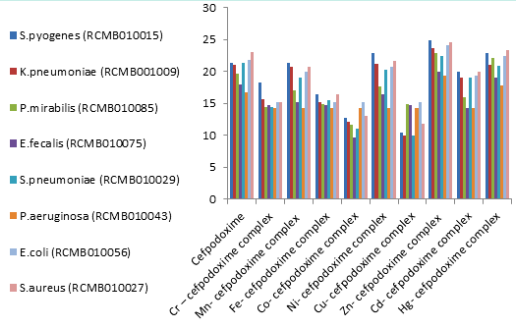

Figure 16: Antifungal activity of cefpodoxime and its metal complexes.

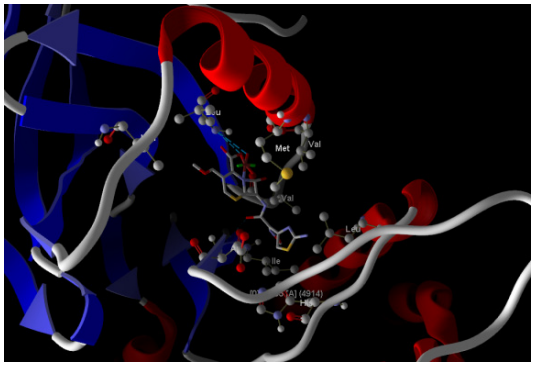

Figure 17: Virtual Molecular docking of the best docked (Zn-complex) with 5GH5 protein.

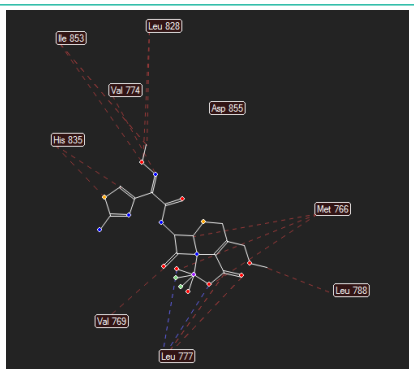

Figure 18: 2D structure of Molecular docking of (Zn-complex) with 5HG5 protein.

and *S. aureus* were subcultured on nutrient agar medium (Oxoid laboratories, UK) for bacteria and sabouraud dextrose agar (Oxoid laboratories, UK) and for fungi while antifungal activities were examined against *A. niger*, *A. flavus*, *S. racemosum*, *C. albicans*, *C. glabrata*, *F. oxysporum*, *R. solani* and *A. solani* fungal strains and. The plates were done in triplicate. Bacterial cultures were incubated at 37°C for 24h, while the other fungal cultures were incubated at (25-30°C) for 3-7 days. Antimicrobial activity was determined by measurement zone of inhibition [11]. The Minimum Inhibitory Concentration (MIC) of the samples was estimated for each of the tested organisms in triplicates. Varying concentrations of the samples (1000-0.007µg/ml), nutrient broth was added and then a loopful of the test organism previously diluted to 0.5 McFarland turbidity standard was introduced to the tubes. A tube containing broth media only was seeded with the test organisms to serve as control. Tubes containing tested organisms' cultures were then incubated at 37°C for 24 h, while the other fungal cultures were incubated at (25-30°C) for 3-7 days. The tubes were then examined for growth by observing for turbidity [12].

Molecular docking: The simulated interaction of designed drug with the protein structure of selected pathogens was modeled by MOE 2015.10 program. The 3D crystal structure of the selected proteins was obtained from the Protein Data Bank (PDB). The inhibition efficiency of the designed drugs is evaluated by the strength of interactions with the target proteins, which was predicted from the scoring energy and the length of the H-bonds in the docked complex. removal of water molecules, atomic charges clarifying, and then energy minimization by MMFF94x force field .10 Poses of interactions were recorded for each species, where the best pose with the shortest ligand-receptor distance and the highest scoring energy is presented in the results and discussion section.

Results and Discussion

IR Spectral Studies

The broad band at 3440 cm^{-1} designated to vO-H engaged in a hydrogen bond is found in the spectrum for the cefpodoxime ligand in Table 2. The C-H stretching vibration bands are similarly present in the 3000 cm-1 range. Due to their overlap with the O-H, these bands either appeared as weak shoulders or as a typical peak. At 500 - 550 cm^{-1}, the metal-oxygen bands associated with rocking modes were visible [13]. The spectrum shows the lactam (C=O) band at 1795 cm^{-1} and the amide (C=O) band at 1635 cm^{-1}.

The prepared complexes showed the lactam carbonyl band at around 1910-1930 cm^{-1} and the amide carbonyl band at range 1635-1654 cm^{-1}. The bands at of 1350 cm^{-1}, corresponding to the COO asymmetrical stretching of the cefpodoxime is shifted to lower wave numbers in the spectra of the complexes, (Cr:1310 cm^{-1}, Mn: 1312 cm^{-1}, Fe:1325 cm^{-1}, Co:1305, Ni:1303 cm^{-1}, Cu:1311 cm^{-1}, Zn:1310 cm^{-1}, Cd:1304 cm^{-1} and Hg:1318 cm^{-1}), indicating coordination through the C=O of the carboxylate group. Thus, cefpodoxime bound as bidentate ligand through both carboxylic and lactam groups. The remaining COO bands, ν_{sym}(COO), γ(COO), ω(COO) and ρ(COO) appeared at 1500, 861, 788 and 640 cm^{-1}, respectively, in cefpodoxime spectrum. The change in positions in the metal complexes spectrum was a result of coordination. The band due to $\nu_{C\text{-}N,}$ of the β-lactam ring (1188 cm^{-1}) is slightly affected on complexation. This is facilitated by appearance of $\nu_{M\text{-}N.}$ In the far IR spectra, the bonding of oxygen is proved by the presence of bands at 480 – 500 cm^{-1} (M-O) [14].

Electronic Spectra and Magnetic Susceptibility Studies

Cr^{III}-cefpodoxime complex, showed four bands at 325, 350, 415, 600 nm, respectively due to charge n→π* of the ligand, $^4A_{2g}\rightarrow{}^4T_{2g}$ (F), $^4A_{2g}\rightarrow{}^4T_{1g}$(F) and $^4A_{2g}\rightarrow{}^4T_{1g}$(p) transitions of the metal. The complex had a magnetic moment of 3.88 B.M, which is expected for octahedral configurations due to spin only of the complexes. Thus, the data indicated that the complex has also the octahedral geometry with high spin state. The electronic absorption spectrum of the Mn^{II}- cefpodoxime complex gave four bands, 305, 350, 400, 450, 528 nm, assigned to $^6A_1(S)\rightarrow{}^4T_2(p)$, $^6A_1(S)\rightarrow{}^6A_1(G)$, $^6A_1(S)\rightarrow{}^4E(G)$, $^6A_1(S)\rightarrow{}^4T_2(G)$ and $^6A_1(S)\rightarrow{}^4T_1(G)$ transitions, indicating the Oh geometry.

The spectrum of this complex resembles the spectra of hydrated Mn^{II} complex where it is characterized by: (a) The weakness of the bands, (b) The large number of the bands, (c) the great variation in the width of the bands, with one band extremely narrow indeed. The electronic absorption spectra of the Fe^{III}-cefpodoxime complex showed two bands at 335, 510 nm. The first band is assigned to be CT while the second broad band is due to $^6T_{2g}\rightarrow{}^5E_g$ transition. However, the room temperature magnetic moment value was found to be 5.95 B.M. The data typified the existence of octahedral configuration in high spin state [15-17]. The electronic absorption spectral bands of the Co^{II}-cefpodoxime complex, gave three bands at 295, 350 and 540 nm. The first two bands are of metal to ligand charge transfer nature and the latter broad bands are assigned to $^4T_{1g}(F)\rightarrow{}^4T_{1g}(P)$ transition. This proved the O_h geometry of the complex [18-20]. The magnetic moment value was found to be 3.85 BM, indicated high spin nature of the complex. The electronic spectra of the Ni^{II}-cefpodoxime complex,gave two bands at 350, 575 nm assigned $^3A_{2g}(F)\rightarrow{}^3T_{1g}(P)$ and $^3A_{2g}(F)\rightarrow{}^3T_{1g}(F)$ transitions. Also, the broadness is attributed to the existence of more than d-d transition overlapped with each other [18-21]. The room temperature magnetic moment value was 2.81 B.M to assign high spin octahedral configuration

The electronic spectra of the Cu^{II}- cefpodoxime complex, gave two bands at 493 and 800 nm, these bands are assumed to be due to $^3B_{1g}\rightarrow{}^2A_{1g}$, and $^3B_{1g}\rightarrow{}^2T_{2g}$(D), respectively. This may be attributed to the distortion of the octahedral due to the drug itself with Jahn-Taller effect. Zinc, cadmium and mercury complexes didn't give visible spectra. All of them were found to be diamagnetic in nature and assumed to be of octahedral geometry like the rest transition metal ions under investigation.

Electron Spin Resonance of Copper Complex

Cu-cefpodoxime complex's room temperature X-band ESR spectral pattern, shown in Figure 2 and Table 4, is anisotropic in nature with g// = 2.0264 and g = 2.263. Weak signals at g = 4 suggested a specific sort of Cu-Cu interaction called spin-spin interaction between Cu atoms. The values were computed using the following equation: The G value for the copper complex was 0.00995, which is significantly less than 4, and it showed that there was very strong contact between copper atoms in the solid state. [22-25] The information demonstrated that both complexes were axially compressed. These findings agree with the magnetic properties that have already been covered. it's possible to measure the covalent bond character α^2, where α is the coefficient of the d_z^2 ground state of orbital, from the expression [26].

Mössbauer- Spectroscopy

Figure 3 shows a doublet of spectral lines with very near (EQ = O.510 and EQ == 0.507 mm/sec.) Mössbauer data of the cefpodoxime-prepared iron complexes. These characteristics match those for high spin FeIII complexes [27]. The calculated isomer shift values match those published for high spin FeIII complexes (between 0.5 and 0.7 mm/sec) [28], which supports the geometry predicted and the previous values of eff for the two complexes.

From the IR data gathered with the electronic spectra, magnetic susceptibility measurements, ESR spectra and *Mössbauer Spectroscopy*, the structures of the prepared complexes collected in Figures 4.

Thermal Analysis

Thermodynamics of complexes of Cefpodoxime's TG and DTA curves, shown in Figures 5, revealed four peaks with orders of 1.26, 1.38, 1.14, and 1.22 and activation energies of 30.65, 87.78, 20.46, and 37.05 kJ/mol, respectively. There is no trace of the dissociation processes. The four stages' S values varied from -0.11 to -0.13 kJ/mol in Table 4, showing that the dissociation steps' transition states were more ordered than their reactants and that all four steps followed the same trend. Table 4 provides the values for H and collision number Z for the dissociation steps. The dissociation's mechanism, Figure 6, is suggested to be removal of 2-amino- 1,3-thiazol, step I then the methoxymethyl, step II then 2-methoxyimino-acetyl amino, step III then thia- 1-azabicyclo [4.2.0] oct- 2-ene in step IV to leave no residue.

Electrical Conductivity Measurements

The information on electrical conductivity is displayed in Figures (7-9) and compiled in Tables (6-7). The data show that all complexes behave like semiconductors. It is possible to argue that the discontinuity in the complexes' conductivity curves results from a chemical rearrangement. This character, who inhabits certain complexes, exhibits semi-conducting behavior. At 0 K, semiconductor materials have insulator-like characteristics.

The conductivity of the Cr-cefpodoxime complex, for instance, revealed three areas with temperature breaks at 28 and 132°C. Temperature causes an increase in conductivity. The ΔEa - $\ln\sigma_o$ curve, Figure (9), gave the following equation for the conduction of chromium cefpodoxime complex: ΔEa = 2.0736. $\ln \sigma_o$ - 0.0005. Similar equations are given for the other studied complexes: Mn- cefpodoxime complex, ΔEa = 1.1138 $\ln \sigma_o - 6x10^{-5}$, Fe-cefpodoxime complex, ΔEa = $3x10^{-05}$ $\ln \sigma_o$ + 0.0005, Co-cefpodoxime complex, ΔEa = 0.9427 $\ln \sigma_o + 2x10^{-5}$, Ni-cefpodoxime complex, ΔEa = 0.9306 $\ln \sigma_o + 3x10^{-5}$, Cu- cefpodoxime complex, ΔEa = $3x10^{-5}$ $\ln \sigma_o$ + 0.0005, Zn- cefpodoxime complex, ΔEa = 0.5746 $\ln \sigma_o$ + 0.0002, Cd- cefpodoxime complex, ΔEa = 0.930 $\ln \sigma_o + 4x10^{-5}$, Hg- cefpodoxime complex, ΔEa = $3x10^{-5}$ $\ln \sigma_o$ + 0.0005

Generally, this data proved the semiconducting behavior of these metal cefpodoxime complexes. The $\ln_o$ and ΔEa values of these complexes are collected in Table (7).

Dielectric Studies

This descriptive study's methodology is based on recording the potential difference, V, the phase angle, q, the dielectric constant, D, and the capacitance, C, at 30°C while varying the frequency from 0.1 to 100 kHz. For the investigated cefpodoxime metal complexes, Figures (10) depict the relationship between frequency and potential. We can claim that there has been a notable change that may be linked to the nature of the ligand in the case of cefpodoxime complexes because Zn and Cd complexes showed the same pattern.

Figure (11) depicts the capacity-frequency relationships for cefpodoxime complexes.

After decreasing, the capacity values stabilize. Regarding how the dielectric constant varies, D, According to Figure (12), the D values for both Zn and Cd cefpodoxime complexes start to rise at law frequencies, and at higher frequencies, the change becomes very minor within a constrained range of D values. The D values for Hg cefpodoxime complex are significantly high at law frequencies before decreasing to the same constrained range as Zn and Cd complex. It is well known that the permittivity value, e, depends on the external variables that are subject to change, specifically the temperature and the frequency of the voltage applied to the dielectric. Additionally, it was noted that when non-polar dielectric permittivity changes within extremely broad bounds and in cases of dipoles, it is not frequency dependent.

Biological Activity

Antibacterial activity: According to Figure (12), the D values for both Zn and Cd cefpodoxime complexes start to rise at law frequencies, and at higher frequencies, the change becomes very minor within a constrained range of D values.

The D values for Hg cefpodoxime complex are significantly high at law frequencies before decreasing to the same constrained range as Zn and Cd complex. It is well known that the permittivity value, e, depends on the external variables that are subject to change, specifically the temperature and the frequency of the voltage applied to the dielectric. Additionally, it was noted that when non-polar dielectric permittivity changes within extremely broad bounds and in cases of dipoles, it is not frequency dependent. The minimum and the maximum value of Fe-cefpodoxime complex were 14.3 and 16.5 for P.aeruginosa and S.aureus, respectively, while that of Cu-cefpodoxime complex were 10 for K.pneumoniae and S.pneumoniae to 15.2 for E.coli, respectively. The MIC values for antibacterial activity are shown in Table (10).

Antifungal Activity

Cefpodoxime and its metal complexes' antifungal effects against the fungi A. niger, A. flavus, S. racemosum, C. albicans, C. glabrata, F. oxysporum, R. solani, and A. solani are shown in Table (11) and Figures (15,16) [32]. The selected complexes' Minimum Inhibitory Concentrations (MIC) were identified and listed in Table (8,9). The results show that the complexes have the potential to be effective fungal organism inhibitors. The largest values of inhibition were recorded to F.oxysporum, (Table 11), while the least values of inhibition were recorded for cefpodoxime, and most of their complexes for the fungi known as R.solani.

Molecular Docking

The Molecular Operating Environmental module MOE2015 software package is used to predict the biological features of candidate drugs and to anticipate the experimental results [33,34]. In the present study, the protein structure of 5HG5 was used as the receptors docked with Zn-complex as inhibitors for lung cancer Figure (17). Docking results include ligand-receptor sites, interaction type, interaction distances (A), internal Energy (E), and scoring energy (S) in kcal/mole. The negative value for energies implies the spontaneous binding of the tested inhibitor to the target protein. The data propose the best interaction stability for docked compounds.

The effective ligand-receptor interaction distances were ≤ 3.5 A in most cases, which indicates the presence of typical real bonds and hence high binding affinity. For example, the nearest interaction is observed via H-donors with 5GH5 (2.72A) and (Zn-complex). With scoring energy (S) -0.0379 kcal/mole Furthermore, the scoring energy function (S) is taken as an indication of high ligand-protein binding affinity based on several factors such as hydrogen bonds, deformation impact, hydrophobicity, entropy, and van der Waals interaction . Furthermore, sex binding sites were observed of different amino acids (His 835, Val 769, Val 774, Leu 777, Leu788, Leu 828, Met 766, Asp 855, and Lle 853) with Zn-complex demonstrating their high inhibition efficacy as candidates, Figure (18).

References

1. Sauer CM, Dong J, Celi LA, Ramazzotti D. Improved Survival of Cancer Patients Admitted to the Intensive Care Unit between 2002 and 2011 at a US Teaching Hospital. Cancer Res Treat. 2019; 51: 973–81.
2. Azoulay E, Mokart D, Kouatchet A, Demoule A, Lemiale V. Acute respiratory failure in immunocompromised adults. Lancet Respira Med. 2019; 7: 173–86.
3. De Giacomi F, Vassallo R, Yi ES, Ryu JH. Acute Eosinophilic Pneumonia. Causes, Diagnosis, and Management. Am J Respir Crit Care Med. 2018; 197: 728–36.
4. Allen JN, Pacht ER, Gadek JE, Davis WB. Acute eosinophilic pneumonia as a reversible cause of noninfectious respiratory failure. N Engl J Med. 1989; 321: 569–74.
5. Gagnier JJ, Kienle G, Altman DG, Moher D, Sox H, Riley D. The CARE guidelines: consensus-based clinical case reporting guideline development. BMJ Case Rep. 2013; 7: 223.

6. Araújo D, Meira L, Moreira C, Morais A. Eosinophilic pneumonia as a paraneoplastic manifestation of colon adenocarcinoma. Archives of bronchopneumology. 2016; 52: 224–5.

7. Amy D. Treatise on internal medicine. Eosinophilic syndromes. 26th ed. Goldman L, Ausiello DA, Schafer AI, editors. Spain: Elsevier. 2021. 1117–1120.

8. Kaul B, Farrand E. Ferri's Clinical Advisor 2024. Eosinophilic Pneumonia. 1st ed. Ferri FF, editor. 2023; 545: E7-545.E10.

9. Fridlender ZG, Simon HU, Shalit M. Metastatic carcinoma presenting with concomitant eosinophilia and thromboembolism. Am J Med Sci. 2003; 326: 98–101.

10. Uemura K, Nakajima M, Yamauchi N, Fukayama M, Yoshida K. Sudden death of a patient with primary hypereosinophilia, colon tumors, and pulmonary embolism. J Clin Pathol. 2004; 57: 541–3.

11. Chang WC, Liaw CC, Wang PN, Tsai YH, Hsueh S. Tumor- associated hypereosinophilia: report of four cases. Changgeng Yi Xue Za Zhi. 1996; 19: 66–70.

12. Yuen BH, Reyes CV, Rawal PA, Sosman J, Jensen J. Severe eosinophilia, and hepatocellular carcinoma: an unusual association. Diagnose Cytopathol. 1995; 13: 151–4.

13. Hirata J, Koga T, Nishimura J, Ibayashi H. Pancreatic carcinoma associated with marked Eosinophilia: a case report. Eur J Haematol. 1987; 39: 462–6.

14. Reddy SS, Hyland RH, Alison RE, Sturgeon JF, Hutcheon MA. Tumor- associated peripheral eosinophilia: two unusual cases. J Clin Oncol. 1984; 2: 1165–9.

15. Scherer TA. Tumor Associated Blood Eosinophilia and Eosinophilic Pleural Effusion: Case Report and Review of the Literature. The Internet Journal of Emergency and Intensive Care Medicine. 1996; 1.

16. Horie S, Okubo Y, Suzuki J, Isobe M. An emaciated man with eosinophilic pneumonia. Lancet. 1996; 348: 166.

17. Hirshberg B, Kramer MR, Lotem M, Barak V, Shustin L, Amir G, et al. Chronicle eosinophilic pneumonia associated with cutaneous T- cell lymphoma. Am J Hematol. 1999; 60: 143–7.

18. Ishiguro T, Kimura H, Araya T, Minato H, Katayama N, Yasui M, et al. Eosinophilic pneumonia and thoracic metastases as yet initial manifestation of prostatic carcinoma. Intern Med. 2008; 47: 1419–23.

19. Kalra A, Fabius D, Gajera M, Palaniswamy C. Triad of Interstitial Pneumonia, Eosinophilia, and Eosinophilic Pleural Effusion: A Rare Paraneoplastic Manifestation of Lung Adenocarcinoma. Chest. 2010; 138: 1–2.

20. Verstraeten AS, De Weerdt A, van Den Eynden G, Van Marck E, Snoeckx A, Jorens PG. excessive eosinophilia as paraneoplastic syndrome in a patient with non - small - cell lung carcinoma: a case report and review of the literature. Clin Belg Act. 2011; 66: 293–7.

21. Paraandavaji E, Hadidi H, Norouzi M, Azaddehghan M, Khodaparasti M, Shafiei S, et al. Paraneoplastic acute eosinophilic pneumonia due to carotid angiosarcoma: A rare case. Vol. 11, Clinical case reports. England. 2023; 11: e7348.

22. Rhee CK, Min KH, Yim NY, Lee JE, Lee NR, Chung MP, et al. Clinical characteristics and corticosteroid treatment of acute eosinophilic pneumonia. Eur Respir J. 2013; 41: 402–9.

23. Simon HU, Plötz SG, Dummer R, Blaser K. Abnormal clones of T cells producing interleukin-5 in idiopathic eosinophilia. N Engl J Med. 1999; 341: 1112–20.

24. Shorr A, Myers J, Huang D, Nathanson B, Emons M, Kollef M. A risk score for identifying patients with eosinophilic pneumonia at high risks for relapse. Chest. 2013; 144: 1917–23.

25. Pahal P, Penmetsa GK, Modi P, Sharma S. Eosinophilic Pneumonia. In Treasure Island (FL). 2023.